The influence of astigmatic aberration on the Gaussian beam diffraction in the near field of axicons and ring gratings

D.A. Savelyev [1,2], P.A. Khorin [1]
[1] Samara National Research University, Moskovskoye Shosse 34, Samara, 443086, Russia;
[2] Image Processing Systems Institute, NRC "Kurchatov Institute",
Molodogvardeiskaya Str. 151, Samara, 443001, Russia

Abstract

The diffraction of Gaussian beams with astigmatic aberration on high–aperture diffractive axicons with different relief heights was studied in this paper. Also the axicons and ring gratings without a central zone were considered. The finite difference time domain method was used for modeling. It is shown that increasing the relief height of the diffractive axicon leads to the formation of the chains of maxima outside the element. The minimum focal spot size outside the element in the presence of astigmatic aberration ($\alpha = 141.68$) in the input beam was observed for the case of an axicon without a central zone for $h = 4.24\lambda$, (FWHM = 0.43λ). The longest light needle was obtained for the same type of beam and element, but at a height of $h = 1.06\lambda$ (DOF = 5.96λ).

Keywords: astigmatic aberration, Gaussian beam, diffractive axicon, ring gratings, FDTD.

Citation: Savelyev DA, Khorin PA. The influence of astigmatic aberration on the Gaussian beam diffraction in the near field of axicons and ring gratings. Computer Optics 2025; 49(6): 1228-1235. DOI: 10.18287/COJ1832.

Acknowledgements: This research was funded by the Russian Science Foundation under grant No. 24–79–10101, https://rscf.ru/en/project/24–79–10101/ (numerical simulation) and within the government project of the National Research Center "Kurchatov Institute" (the part Introduction).

Introduction

It is well known that a real lens always introduces distortions when forming an image [1 – 3]. One of the causes of distortions are various types of aberrations, such as coma, distortion, astigmatism, and others [1, 2]. Reduction and compensation of optical aberrations is an urgent problem solved by adaptive optics [1, 4 – 6], the use of which allows obtaining high–quality images of biological structures in complex tissues and medical diagnostics [3, 6 – 8], images of exoplanets in astronomy [1, 9], compensating for chromatic aberrations [10], including in the development of virtual reality headsets [11], contact lenses [12]. It is known to use methods based on artificial intelligence for detection, compensation and recognition[13 – 18], in particular, to compensate for phase aberrations in digital holography [16, 18]. It should also be noted that a number of defects of optical systems could be described by wavefront aberrations [19 – 21].

Diffractive optical elements (DOE) [22 – 29] are distinguished by their versatility and efficiency when used in such areas as optical communications, holography, formation of the required distribution of laser beams, visualization systems, and compensation for aberrations of optical systems [22]. Formation of a complex spatial distribution during generation of the second harmonic of a Bessel–Gauss beam by axicons with asymmetric aberrations is known [23]. It should also be noted that in the case of subwavelength dimensions of elements, it is important to take into account the height of individual relief elements [26, 29, 30].

Gaussian beams have not lost their relevance to this day when solving problems in photonics and optics [30 – 42], in particular, when forming long optical needles [35, 36] and optical bottles [26, 30], sharp focusing [33, 36], and other areas of optics [38]. There are also known works on the propagation of Gaussian beams in various media, in particular, under conditions of anisotropic turbulence [31].

The propagation features of Gaussian beams with introduced astigmatic aberration on ring gratings at different relief heights examines in this paper. Numerical modeling was performed using the finite difference time domain (FDTD) method [43] using software Meep [44 – 46].

1. The simulation parameters and input beams

The following simulation parameters were used in the paper: the input radiation wavelength $\lambda = 0.532$ μm. A three–dimensional computational domain was considered, where $x, y, z \in [0, 15.8\lambda]$. This domain was surrounded by an absorbing layer *PML* (1.1λ) on all sides. The spatial simulation step was $\lambda/50$, the time simulation step was $\lambda/(100c)$, where c is the speed of light. The fundamental Gaussian mode (beam size $\sigma = 1.5$ μm) with circular polarization was considered as the input beam, supplemented with an astigmatic aberration of the form $\exp(i\alpha xy/R^2)$, where R – is the radius of the considered domain, α is a parameter corresponding to the value of aberration. Examples of input beams propagating in free space outside the element are shown in Fig. 1 ($\alpha = 0$, 35.99, 71.98, 107.98, 141.68).

The diffractive axicons and ring gratings with numerical aperture $NA = 0.95$ and refractive index $n = 1.47$ were considered as an optical elements, where $NA = \lambda / d$ (d – period of the axicon and the ring grating, $d = 1.05\lambda$).

The relief heights of this elements h corresponded to a phase jump of π radians ($h = 1.06\lambda$), as well as multiples of this value: 2π ($h = 2.12\lambda$), 3π ($h = 3.18\lambda$) and 4π ($h = 4.24\lambda$) radians. A study was also conducted on the passage of the considered laser beams through axicons with a similar height, but without a central zone.

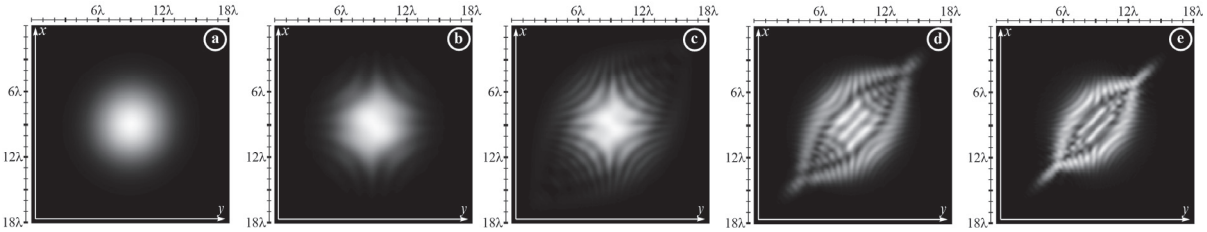

Fig. 1. The input beams, at different values of α, intensity: a) α = 0, b) α = 35.99, c) α = 71.98, d) α = 107.98, e) α = 141.68

The diffraction patterns of the Gaussian beam propagation (α = 0) through the diffraction axicons are shown in Fig. 2 (with a central zone) and Fig. 3 (without a central zone)

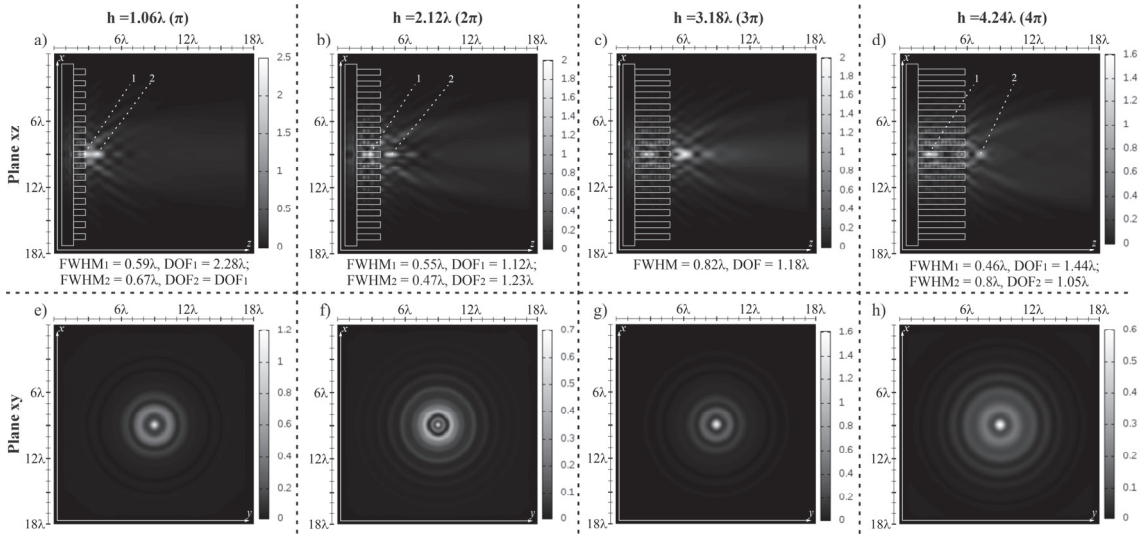

Fig. 2. Two–dimensional diffraction pattern (intensity) of a standard Gaussian beam (α = 0) at different axicon relief heights, xz plane (a, b, c, d) and in the xy plane at a distance S = 1.5λ (e, f, g, h)

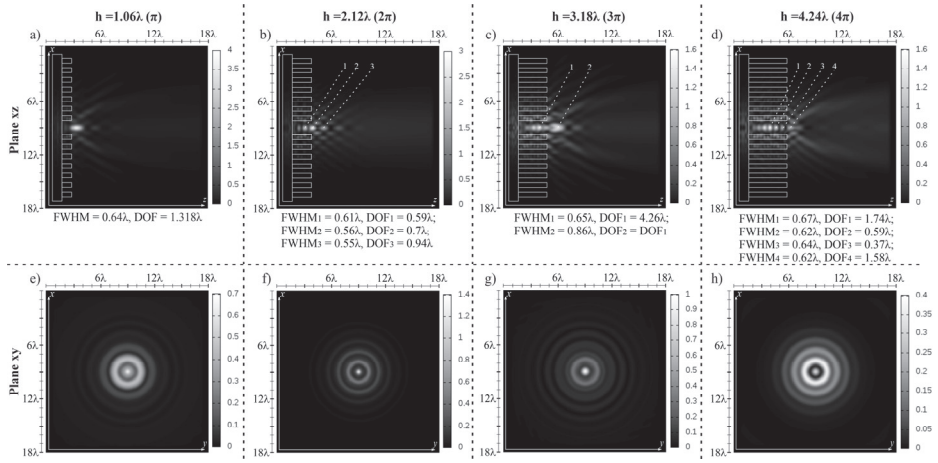

Fig. 3. Two–dimensional diffraction pattern (intensity) of a standard Gaussian beam (α = 0) at different relief heights of the axicon without a central zone, in the xz plane (a, b, c, d) and in the xy plane (e, f, g, h), the sections in the xy plane were considered at a distance S = 1.5λ

The focal spot size in the transverse region was estimated as the full width at half maximum (FWHM) intensity, in the longitudinal region the light needle size was estimated similarly (depth of focus, DOF). The values are given for the global maximum on the optical axis and the maximum outside the element. In the case of several maxima, their locations are indicated by numbers in the figures. Transverse diffraction patterns (xy plane) were considered at the same distance from the edge of the relief of the elements $S = 1.5\lambda$ in all cases considered in the paper.

The following should be noted with analyzing Fig. 2: only for the case of $h = 3.18\lambda$ there is the formation of the main maximum outside the relief of the element observed at a distance of $S = 1.2\lambda$. In the other cases, the main maxima are

formed inside the element, although for the case of $h = 1.06\lambda$ this occurs, in fact, at the boundary, at a distance of 0.07λ from the edge of the relief (Fig. 2*a*). It should also be noted that outside the relief in all the cases, a decrease in the intensity of the second maximum (outside the relief) of the element is observed.

Let I – be the intensity value from the maximum value on the optical axis, which is 100 %. Then, at $h = 1.06\lambda$, the maximum outside the element is $I = 97.73$ %, at $h = 2.12\lambda$, for the maximum outside the element, $I = 87.6$ %, and for $h = 4.24\lambda$, the maximum outside the element is $I = 71.9$ %. The minimum focal spot size outside the element was obtained for the case $h = 2.12\lambda$ (FWHM = 0.47λ), the maximum light needle – for the case $h = 1.06\lambda$ (DOF = 2.28λ).

If we remove the central zone, the maximum will be formed outside the element. For the height $h = 1.06\lambda$, one main maximum is observed on the optical axis in contrast to the previously considered case. A further increase in the relief height leads to the formation of a chain of foci on the optical axis, which is especially noticeable for the case of $h = 4.26\lambda$. We will separately note the case of $h = 3.18\lambda$, when the formation of a light needle with a length of DOF = 4.26λ is observed.

2. The Gaussian beam with astigmatic aberration and ring gratings height changing

This section considers the cases when $\alpha = 35.99, 71.98, 107.98, 141.68$. The diffraction patterns for the propagation of Gaussian beams with astigmatic aberration through the previously considered diffraction axicons are shown in Fig. 4.

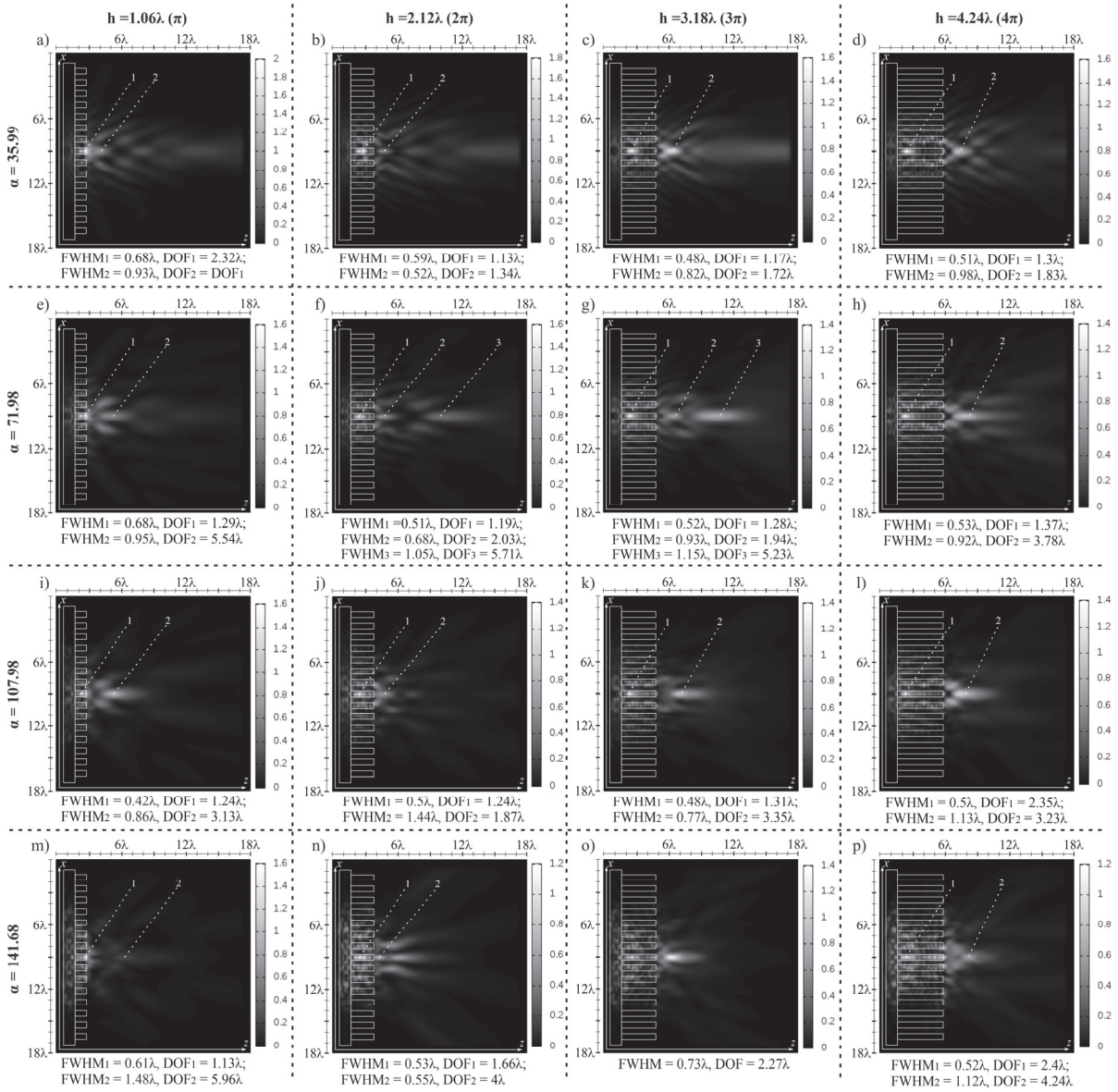

Fig. 4. Two–dimensional diffraction pattern (intensity, xz plane) of Gaussian beams for different values of α (35.99, 71.98, 107.98, 141.68) at the height of the ring grating h = 1.06λ (a, e, i, m), h = 2.12λ (b, f, j, n), h = 3.18λ (c, g, k, o), h = 4.24λ (d, h, l, p)

It should be noted that the main maxima are formed inside the element as before, only for the case of $h = 3.18\lambda$ at $\alpha = 141.68$ (Fig. 4*o*) the formation of the main maximum is observed outside the ring grating with FWHM = 0.73λ and DOF = 2.27λ.

The main maximum is formed inside the relief for the height $h = 1.06\lambda$ on the boundary, within 0.07λ for the cases $\alpha = 35.99$, 71.98, 141.68, but for the case $\alpha = 107.98$, the main maximum is formed already at a distance of 0.42λ.

The intensity value of the maxima on the optical axis is generally significantly smaller in contrast to the case of a standard Gaussian beam without distortions: in half of the cases considered in Fig. 4, $I < 70\,\%$. Only in two cases is observed $I > 90\,\%$, at $h = 3.18\lambda$ and $\alpha = 35.99$ ($I = 91.2\,\%$, Fig. 4*c*), and at $h = 4.26\lambda$ and $\alpha = 107.98$ ($I = 90.9\,\%$, Fig. 4*l*). However, for all considered α in the case of height $h = 4.26\lambda$, the value of the maximum outside the element is $I > 70\,\%$.

The minimum focal spot size outside the element was obtained for the case of $h = 2.12\lambda$, $\alpha = 35.99$ (FWHM = 0.52λ, $I = 56.7\,\%$, Fig. 4*b*), light needles larger than 5λ were obtained for the cases of $h = 1.06\lambda$, $\alpha = 141.68$ (DOF = 5.96λ, $I = 29.6\,\%$, Fig. 4*m*); $h = 1.06\lambda$, $\alpha = 71.98$ (DOF = 5.54λ, $I = 57.8\,\%$, Fig. 4*e*); and $h = 3.18\lambda$, $\alpha = 71.98$ (DOF = 5.23λ, $I = 68.4\,\%$, Fig. 4*g*).

However, the longitudinal section does not provide complete information about the diffraction patterns formed. Let us also consider the cross sections, as before, at a distance of 1.5λ (Fig. 5).

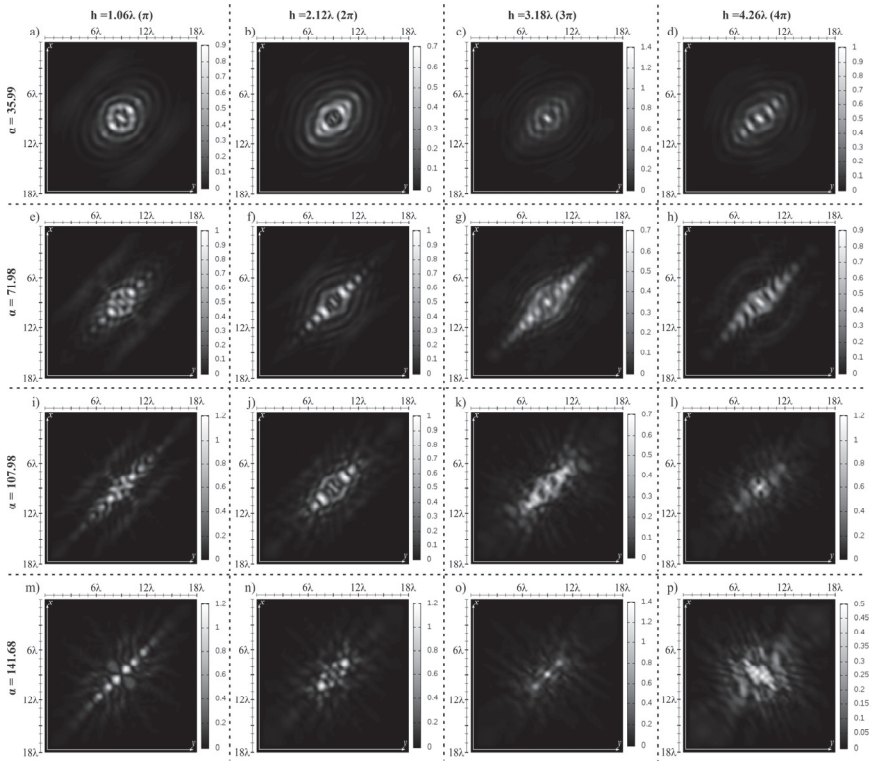

Fig. 5. The sections in the xy plane (intensity) at a distance $S = 1.5\lambda$, with $\alpha = 35.99$ (a, b, c, d), $\alpha = 71.98$ (e, f, g, h), $\alpha = 107.98$ (i, j, k, l), $\alpha = 141.68$ (m, n, o, p)

It should be noted that for the case of $h = 3.18\lambda$ (for all considered α) the formation of a light spot is observed on the optical axis, and for $\alpha = 141.68$ it is the least distorted.

A focal spot of comparable size is also observed for the case of $h = 4.26\lambda$ and $\alpha = 107.98$.

3. The Gaussian beam with astigmatic aberration and ring gratings height changing without the central zone

It was shown earlier that the main maxima are mainly formed inside the optical element. As before, we will change the height of the elements, but without the central zone.

The obtained intensity distributions during the propagation of Gaussian beams with astigmatic aberration through ring grating without a central zone are shown in Fig. 6, and the transverse intensity distribution patterns in the xy plane at a distance of $S = 1.5\lambda$ are shown in Fig. 7.

In all cases, the main maximum is formed outside the relief of the axicons, and also outside the height of the relief of the element rings.

For the height $h = 1.06\lambda$ one main maximum is observed on the optical axis as for the Gaussian beam at $\alpha = 0$, in contrast to the two maxima of the previous section at a similar element height. Increasing the height of the element rings leads to the formation of chains of foci on the optical axis. For the case of $\alpha = 71.98$ at a height of $h = 2.12\lambda$ (Fig. 6*f*), the formation of two optical bottles is observed.

The minimum focal spot size was obtained for the case of $h = 4.24\lambda$, $\alpha = 141.68$ (FWHM = 0.43λ, $I = 100\,\%$, Fig. 6*p*), and light needles larger than 4 λ were observed for the cases of $h = 3.18\lambda$, $\alpha = 71.8$ (DOF = 5.01λ, $I = 71.1\,\%$, Fig. 6*g*), $h = 1.06\lambda$, $\alpha = 107.98$ (DOF = 4.86λ, $I = 100\,\%$, Fig. 6*i*) and $h = 2.12\lambda$, $\alpha = 71.98$ (DOF = 4.44λ, $I = 73.2\,\%$, Fig. 6*f*).

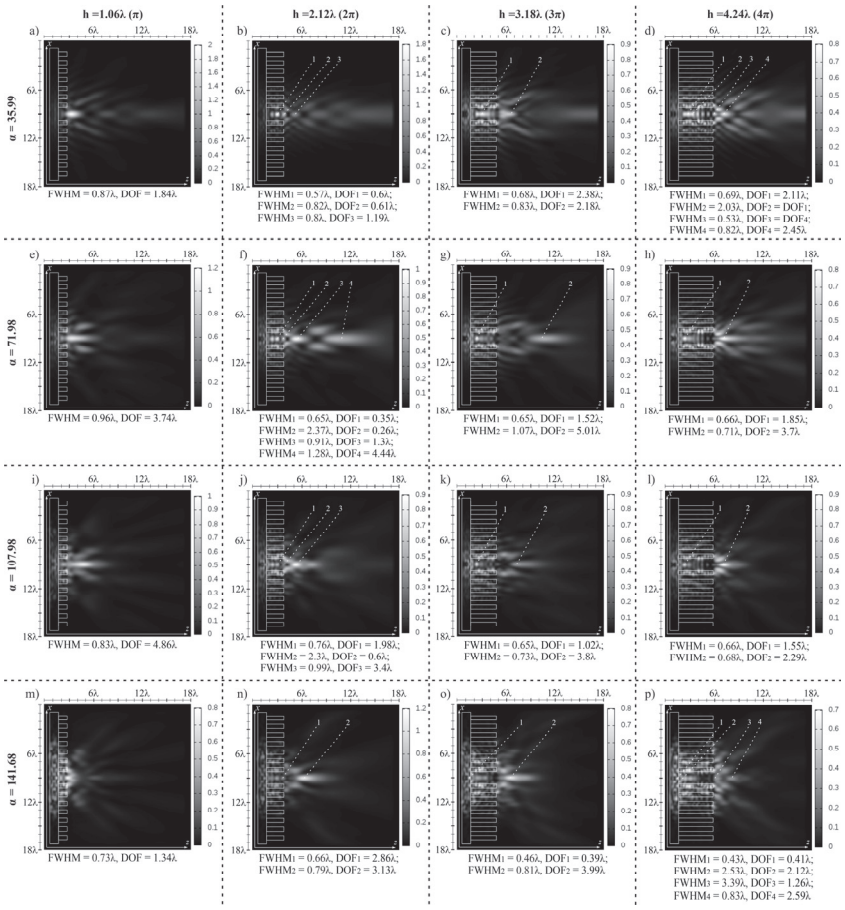

Fig. 6. Two–dimensional diffraction pattern (intensity, xz plane) of Gaussian beams at different values of α (35.99, 71.98, 107.98, 141.68) at the height of the ring grating without the central zone h = 1.06λ (a, e, i, m), h = 2.12λ (b, f, j, n), h = 3.18λ (c, g, k, o) and h = 4.24λ (d, h, l, p)

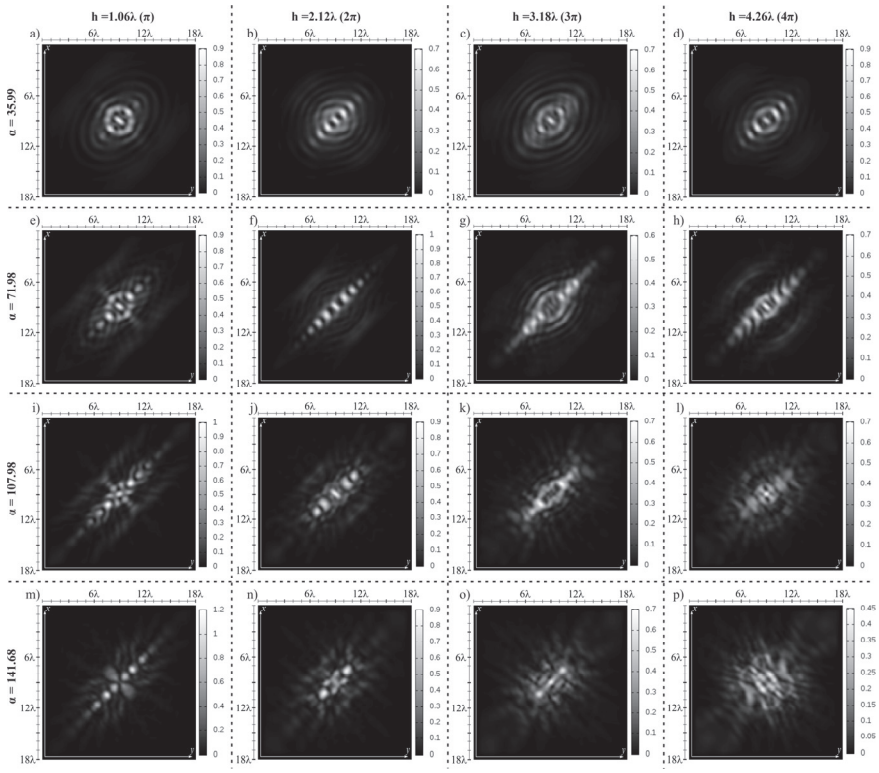

Fig. 7. The sections in the xy plane (intensity) at a distance S = 1.5λ, with α = 35.99 (a, b, c, d), α = 71.98 (e, f, g, h), α = 107.98 (i, j, k, l), α = 141.68 (m, n, o, p), ring grating without central zone)

It should be noted that the formation of more extended light needles was observed when using elements without a central zone than in its presence for all types of beams. Despite the smaller dimensions of the light segments on the optical axis, the intensity values were generally higher than in the presence of a central zone in the subwave axicon.

Conclusion

The FDTD method was used to study the diffraction of Gaussian beams with astigmatic aberration under circular polarization on diffraction axicons with and without a central zone for different relief heights of elements in this paper. The relief heights of the elements were chosen as multiples of the phase jump of π radians. It was shown that an increase in the relief height leads to the formation of chains of maxima outside the element.

The minimum focal spot size of Gaussian beam without aberrations was obtained for the case of $h = 2.12\lambda$ (FWHM = 0.47λ), the maximum light needle – for the case of $h = 1.06\lambda$ (DOF = 2.28λ).

The minimum focal spot size outside the element in the presence of astigmatic aberration was observed for the case of an axicon without a central zone for $h = 4.24\lambda$, $\alpha = 141.68$ (FWHM = 0.43λ), the longest light needle (in the presence of astigmatic aberration) was obtained for the case of $h = 1.06\lambda$, $\alpha = 141.68$ (DOF = 5.96λ).

Acknowledgements

This research was funded by the Russian Science Foundation under grant No. 24–79–10101, https://rscf.ru/en/project/24–79–10101/ (numerical simulation) and within the government project of the National Research Center "Kurchatov Institute" (the part Introduction).

References

[1] Booth M, Andrade D, Burke D, Patton B, Zurauskas M. Aberrations and adaptive optics in super–resolution microscopy. Microscopy 2015; 64(4): 251–261. DOI: 10.1093/jmicro/dfv033.

[2] Del Águila-Carrasco AJ, Kruger PB, Lara F, López-Gil N. Aberrations and accommodation. Clinical and Experimental Optometry 2020; 103(1): 95–103. DOI: 10.1111/cxo.12938.

[3] Zhang Q, Hu Q, Berlage C, Kner P, Judkewitz B, Booth M, Ji N. Adaptive optics for optical microscopy. Biomedical Optics Express 2023; 14(4): 1732–1756. DOI: 10.1364/BOE.479886.

[4] Hampson KM, Turcotte R, Miller DT, Kurokawa K, Males JR, Ji N, Booth MJ. Adaptive optics for high–resolution imaging. Nature Reviews Methods Primers 2021; 1(1): 68. DOI: 10.1038/s43586–021–00066–7.

[5] Marcos S, Artal P, Atchison DA, Hampson K, Legras R, Lundström L, Yoon G. Adaptive optics visual simulators: a review of recent optical designs and applications. Biomedical Optics Express 2022; 13(12): 6508–6532. DOI: 10.1364/BOE.473458.

[6] Wang J, Zhang Y. Adaptive optics in super–resolution microscopy. Biophysics Reports 2021; 7(4): 267. DOI: 10.52601/bpr.2021.210015.

[7] Khorin PA, Khonina SN. Simulation of the Human Myopic Eye Cornea Compensation Based on the Analysis of Aberrometric Data. Vision 2023; 7: 21. DOI: 10.3390/vision7010021.

[8] Zhao J, Zhang Z, Yang Y, Zhang H, Chen H, Wang S, Dai Y. Compact and aberration effects–shielded objective intraocular scatter measurement system. Biomedical Optics Express 2025; 16(2): 669–678. DOI: 10.1364/BOE.545245.

[9] Ashcraft JN, Dube BD, Douglas ES, Kim D, Krist JE, Mennesson B, Monacelli B, Morgan R, Raouf NA, Eldorado Riggs AJ, Rodgers M, Warfield KR. Comparison of polarization aberrations from existing mirror coatings for coronagraphic imaging of habitable worlds. Journal of Astronomical Telescopes, Instruments, and Systems 2025; 11(1): 015002. DOI: 10.1117/1.JATIS.11.1.015002.

[10] Gawne TJ, Banks MS. The Role of Chromatic Aberration in Vision. Annual Review of Vision Science 2024; 10: 199–212. DOI: 10.1146/annurev–vision–101222–052228.

[11] Peng WJ, Lee TX. Mitigating chromatic aberration in wide–field pancake VR optics through the integration of diffractive optical elements. Optics Continuum 2025; 4(1): 37–58. DOI: 10.1364/OPTCON.545381.

[12] Suliman A, Rubin A. A review of higher order aberrations of the human eye. African Vision and Eye Health 2019; 78(1): a550. DOI: 10.4102/aveh.v78i1.501.

[13] Wang H, Lyu M, Situ G. eHoloNet: a learning–based end–to–end approach for in–line digital holographic reconstruction. Optics Express 2018; 26(18): 22603–22614. DOI: 10.1364/OE.26.022603.

[14] Dzyuba AP, Khorin PA, Serafimovich PG, Khonina SN. Wavefront Aberrations Recognition Study Based on Multi–Channel Spatial Filter Matched with Basis Zernike Functions and Convolutional Neural Network with Xception Architecture. Optical Memory and Neural Networks 2024; 33: S53–S64. DOI: 10.3103/S1060992X24700309.

[15] Nguyen T, Bui V, Lam V, Raub CB, Chang LC, Nehmetallah G. Automatic phase aberration compensation for digital holographic microscopy based on deep learning background detection. Optics Express 2017; 25(13): 15043–15057. DOI: 10.1364/OE.25.015043.

[16] Sirico DG, Miccio L, Wang Z, Memmolo P, Xiao W, Che L, Xin L, Pan F, Ferraro P. Compensation of aberrations in holographic microscopes: main strategies and applications. Applied Physics B 2022; 128(4): 78. DOI: 10.1007/s00340–022–07798–8.

[17] Li D, Li Z, Ding W, Wu S, Zhao B, Wang F, Guo R. Simultaneous phase aberration compensation and denoising for quantitative phase imaging in digital holographic microscopy with deep learning. Applied Optics 2024; 63(26): 6931–6940. DOI: 10.1364/AO.534430.

[18] Xiao W, Xin L, Cao R, Wu X, Tian R, Che L, Sun L, Ferraro P, Pan F. Sensing morphogenesis of bone cells under microfluidic shear stress by holographic microscopy and automatic aberration compensation with deep learning. Lab on a Chip 2021; 21(7): 1385–1394. DOI: 10.1039/D0LC01113D.

[19] Chen Z, Leng R, Yan C, Fang C, Wang Z. Analysis of Telescope Wavefront Aberration and Optical Path Stability in Space Gravitational Wave Detection. Applied Sciences 2022; 12(24): 12697. DOI: 10.3390/app122412697.
[20] Romanova GE, Nguyen NS. Third–order aberration analysis of the Fresnel lens. Computer Optics 2023; 47(4): 567–571. DOI: 10.18287/2412–6179–CO–1276.
[21] Klebanov IM, Karsakov AV, Khonina SN, Davydov AN, Polyakov KA. Wavefront aberration compensation of space telescopes with telescope temperature field adjustment. Computer Optics 2017; 41(1): 30–36. DOI: 10.18287/0134–2452–2017–41–1–30–36.
[22] Khonina SN, Kazanskiy NL, Skidanov RV, Butt MA. Advancements and applications of diffractive optical elements in contemporary optics: A comprehensive overview. Advanced Materials Technologies 2025; 10(4): 2401028. DOI: 10.1002/admt.202401028.
[23] Wang T, Buldt F, Bassène P, Reza SBA, Fohtung E, Searles TA, Law CT, N'Gom M. Second harmonic Bessel–Gauss beam shaping with elliptic axicon aberrations. Physical Review Research 2025; 7(1): 013012. DOI: 10.1103/PhysRevResearch.7.0130.
[24] Savelyev DA, Karpeev SV. Development of 3D Microstructures for the Formation of a Set of Optical Traps on the Optical Axis. Photonics 2023; 10(2): 117. DOI: 10.3390/photonics10020117.
[25] Zhang Q, He Z, Xie Z, Tan Q, Sheng Y, Jin G, Cao L, Yuan X. Diffractive optical elements 75 years on: from micro–optics to metasurfaces. Photonics Insights 2023; 2(4): R09. DOI: 10.3788/PI.2023.R09.
[26] Savelyev DA. Peculiarities of focusing circularly and radially polarized super–Gaussian beams using ring gratings with varying relief height. Computer Optics 2022; 46(4): 537–546. DOI: 10.18287/2412–6179–CO–1131.
[27] Siemion A. The magic of optics–an overview of recent advanced terahertz diffractive optical elements. Sensors 2020; 21(1): 100. DOI: 10.3390/s21010100.
[28] Khonina SN, Kazanskiy NL, Khorin PA, Butt MA. Modern types of axicons: new functions and applications. Sensors 2021; 21(19): 6690. DOI: 10.3390/s21196690.
[29] Savelyev DA. Features of focusing of optical vortices using subwavelength elements with varying height of odd and even relief zones. Computer Optics 2024; 48(6): 868–877. DOI: 10.18287/2412–6179–CO–1531.
[30] Savelyev DA. Features of a Gaussian beam near–field diffraction upon variations in the relief height of subwavelength silicon optical elements. Computer Optics 2023; 47(6): 938–947. DOI: 10.18287/2412–6179–CO–1402.
[31] Adams E, van Iersel M. Gaussian beam propagation through anisotropic turbulence: a comparison of the extended Huygens–Fresnel principle and the perturbation method. Journal of the Optical Society of America A 2025; 42(4): 422–432. DOI: 10.1364/JOSAA.554660.
[32] Chalil JG, Kadam S, Joseph C, Kulkarni KJ, Raj AB. Characterization of Free–space Gaussian Beam Propagation and Recent Developments of FSO Communication Technology: A Review. International Journal of Engineering Research and Reviews 2024; 12(3): 1–24. DOI: 10.5281/zenodo.13318940.
[33] Yew EY, Sheppard CJ. Tight focusing of radially polarized Gaussian and Bessel–Gauss beams. Optics Letters 2007; 32(23): 3417–3419. DOI: 10.1364/OL.32.003417.
[34] Levy U, Silberberg Y, Davidson N. Mathematics of vectorial Gaussian beams, Advances in Optics and Photonics 2019; 11(4): 828–891. DOI: 10.1364/AOP.11.000828.
[35] Savelyev DA. The investigation of Gaussian beams and optical vortices diffraction in the near zone of subwavelength optical elements with variable height. Journal of Siberian Federal University Mathematics and Physics 2025; 18(3): 358–370. EDN: NXGRGO.
[36] Shi C, Xu Z, Nie Z, Xia Z, Dong B, Liu J. Sub–wavelength longitudinally polarized optical needle arrays generated with tightly focused radially polarized Gaussian beam. Optics Communications 2022; 505: 127506. DOI: 10.1016/j.optcom.2021.127506.
[37] Azizkhani R, Hebri D, Rasouli S. Gaussian beam diffraction from radial structures: detailed study on the diffraction from sinusoidal amplitude radial gratings. Optics Express 2023; 31(13): 20665–20682. DOI: 10.1364/OE.489659.
[38] Park B, Lee H, Jeon S, Ahn J, Kim HH, Kim C. Reflection-mode switchable subwavelength Bessel-beam and Gaussian-beam photoacoustic microscopy in vivo. Journal of Biophotonics 2019; 12(2): e201800215. DOI: 10.1002/jbio.201800215.
[39] Savelyev DA, Khonina SN, Golub I. Tight focusing of higher orders Laguerre–Gaussian modes. AIP Conference Proceedings 2016; 1724: 020021. DOI: 10.1063/1.4945141.
[40] Ebrahim AAA, Saad F, Belafhal A. Periodic characteristics of a finite Airy–Hermite–Hollow Gaussian beam propagating in a gradient–index medium. Optical and Quantum Electronics 2024; 56(9): 1475. DOI: 10.1007/s11082–024–07378–4.
[41] Chen X, Zhu W, Qian X, Wu P, Wei H, Weng N, Min L, Cui X. Scaling laws for high energy Gaussian beams propagation through the atmosphere. Optics Express 2024; 32(19): 32718–32731. DOI: 10.1364/OE.534378.
[42] Saad F, Benzehoua H, Belafhal A. Evolution properties of Laguerre higher order cosh–Gaussian beam propagating through fractional Fourier transform optical system. Optical and Quantum Electronics 2024; 56(5): 798. DOI: 10.1007/s11082–024–06520–6.
[43] Teixeira FL, Sarris C, Zhang Y, Na DY, Berenger JP, Su Y, Okoniewski M, Chew WC, Backman V, Simpson JJ. Finite–difference time–domain methods. Nature Reviews Methods Primers 2023; 3(1): 75. DOI: 10.1038/s43586–023–00257–4.
[44] Oskooi AF, Roundy D, Ibanescu M, Bermel P, Joannopoulos JD, Johnson SG. MEEP: A flexible free–software package for electromagnetic simulations by the FDTD method. Computer Physics Communications 2010; 181(3): 687–702. DOI: 10.1016/j.cpc.2009.11.008.
[45] Hammond AM, Oskooi A, Chen M, Lin Z, Johnson SG, Ralph SE. High–performance hybrid time/frequency–domain topology optimization for large–scale photonics inverse design. Optics Express 2022; 30(3): 4467–4491. DOI: 10.1364/OE.442074.
[46] Hanson JC. Broadband rf phased array design with meep: Comparisons to array theory in two and three dimensions. Electronics 2021; 10(4): 415. DOI: 10.3390/electronics10040415.

About authors

Dmitry Andreevich Savelyev, associate professor and senior scientist of Samara National Research University (Department of Engineering Cybernetics, Science and Research Laboratory of Automated Systems of Science Researches), junior researcher at the laboratory of laser measurements of the Image Processing Systems Institute, NRC "Kurchatov Institute". Candidate of Physical and Mathematical Sciences. Research interests: diffractive optics, optical and digital image processing, nanophotonics, singular optics, near field optics, polarization transformations, high–performance computing, data science, neural networks. E–mail: *dmitrey.savelyev@yandex.ru*

Pavel Alekseevich Khorin, Candidate of Physical and Mathematical Sciences; Senior researcher of Samara National Research University. Fellowship researcher of ITMO University, Senior researcher of Saint–Petersburg State University. Research interests: mathematical modeling, diffractive optics, optical and digital image processing. E–mail: *paul.95.de@gmail.com / khorin.pa@ssau.ru*

Code of State Categories Scientific and Technical Information (in Russian – GRNTI): 29.31.15
Received February 15, 2025. The final version – October 23, 2025.